

NASA TECHNICAL NOTE



NASA TN D-6268

c. 1

NASA TN D-6268

LOAN COPY: RETURN
AFWL (DOGL)
KIRTLAND AFB, N.



PRELIMINARY THERMAL PERFORMANCE
ANALYSIS OF THE SOLAR BRAYTON
HEAT RECEIVER

by *Raymond K. Burns*
Lewis Research Center
Cleveland, Ohio 44135

NATIONAL AERONAUTICS AND SPACE ADMINISTRATION • WASHINGTON, D. C. • MARCH 1971





0133069

1. Report No. NASA TN D-6268		2. Government Accession No.		3. Recipient's Catalog No.	
4. Title and Subtitle PRELIMINARY THERMAL PERFORMANCE ANALYSIS OF THE SOLAR BRAYTON HEAT RECEIVER				5. Report Date March 1971	
7. Author(s) Raymond K. Burns				6. Performing Organization Code	
9. Performing Organization Name and Address Lewis Research Center National Aeronautics and Space Administration Cleveland, Ohio 44135				8. Performing Organization Report No. E-6042	
12. Sponsoring Agency Name and Address National Aeronautics and Space Administration Washington, D. C. 20546				10. Work Unit No. 128-70	
15. Supplementary Notes				11. Contract or Grant No.	
16. Abstract <p>A thermal performance analysis was performed on the solar Brayton heat receiver. The solar heat receiver, a combination heat exchanger and heat storage device, is designed to transfer 40 kilowatts of heat to the working gas of a Brayton engine. During a sun period of an Earth orbit, a parabolic collector is used to focus solar radiation into the receiver. Excess input solar energy is stored as heat of fusion of lithium fluoride and is withdrawn by the Brayton cycle during shade periods. The analysis predicted an acceptable variation in outlet gas temperature between 1490^o and 1550^o F (1080 and 1120 K) for a nominal design value of 1500^o F (1089 K).</p>				13. Type of Report and Period Covered Technical Note	
17. Key Words (Suggested by Author(s)) Brayton Solar energy Heat exchanger Space power Heat storage				14. Sponsoring Agency Code	
18. Distribution Statement Unclassified - unlimited				15. Supplementary Notes	
19. Security Classif. (of this report) Unclassified		20. Security Classif. (of this page) Unclassified		21. No. of Pages 41	
				22. Price* \$3.00	

PRELIMINARY THERMAL PERFORMANCE ANALYSIS OF THE SOLAR
BRAYTON HEAT RECEIVER

by Raymond K. Burns

Lewis Research Center

SUMMARY

The solar Brayton concept utilizes solar energy for the heat source in a closed-loop Brayton cycle to develop auxiliary electrical power in space. The solar receiver is a combination heat exchanger and heat storage device which transfers 40 kilowatts of heat to a Brayton cycle working gas during both sun and shade periods of an Earth orbit. During a sun period, a parabolic collector is used to focus solar radiation into the receiver through a small aperture located at the collector focal point. The solar input rate is greater than that required for Brayton power system operation during a sun period. The excess energy is stored within the receiver as heat of fusion of lithium fluoride and is then withdrawn during the following shade period to maintain power system operation. Sufficient lithium fluoride is included in the receiver to allow power system operation for shade periods of up to 38 minutes.

A thermal performance analysis of the solar receiver was performed. A digital computer analysis was used to predict the receiver outlet gas temperature as a function of time during an orbit for various combinations of sun and shade period lengths and for various values of radiation properties of the receiver surfaces. The effect of the use of the heat rejection doors, which are movable doors in the receiver insulation used for temperature control, was included in the analysis.

The analysis predicted an acceptable variation in outlet gas temperature, the gas falling below the nominal design value of 1500^o F (1089 K) at the end of a shade period and rising above it at the end of a sun period. In most cases, the gas temperature decrease during the shade period was due to local complete freezing of the lithium fluoride near the beginning of the heated length of the gas flow. Near the end of each sun period some of the lithium fluoride was predicted to locally completely melt and superheat, resulting in the rise in outlet gas temperature. The results indicate that the outlet gas temperature variation during an orbit can be held within the range 1490^o to 1550^o F (1080 to 1120 K). The results show that the receiver thermal performance is sensitive to changes in solar absorptivity of the surfaces and relatively insensitive to changes in emissivity of those surfaces.

INTRODUCTION

A Brayton cycle power system for generation of auxiliary electrical power in space is currently being developed by NASA Lewis Research Center (see refs. 1 and 2). One heat source which has been considered for this system is solar energy. The solar Brayton heat receiver is a combination heat exchanger and heat storage device which transfers energy to a Brayton cycle working gas during both the sun and shade periods of an Earth orbit. During a sun period, a parabolic collector is used to focus solar radiation into the heat receiver through a small aperture located at the collector focal point. The solar input is greater than that required to heat the working gas to the design outlet temperature. Lithium fluoride (LiF) is included in the receiver as an energy storage media. The excess solar energy input during a sun period is stored as heat of fusion in the LiF and is then withdrawn by the working gas during the following shade period. If the orbit is such that the excess solar energy available for storage during a sun period is much in excess of the energy requirements during the following shade period, energy can be rejected to space by opening doors in the insulated walls of the receiver. These heat rejection doors can be opened as required to minimize the time variations in receiver temperature distribution and in receiver outlet gas temperature.

In general, the temperature distribution of the heat receiver and of the receiver outlet gas will vary in time depending on the gas flow rate and inlet temperature, on the solar input rate, on the rate of energy losses through the aperture and through the insulation, on the lengths of the sun and shade periods, and on the use of the heat rejection doors. It is the purpose of the following analysis to determine the performance, characterized primarily by outlet gas temperature, of the present design of the solar heat receiver (designed and fabricated under contract NAS3-10944) for variations of the aforementioned parameters.

Since a design objective for the solar receiver was to minimize time variations in temperature, the first step taken in the analysis was to assume that the receiver was constantly and uniformly at the LiF phase change temperature and to perform an overall heat balance. In this way an estimate of the maximum tolerable insulation losses was obtained as a function of sun and shade period lengths. Near Earth circular orbits of various inclinations and altitudes were then examined to show that the receiver is suitable for use in a wide range of orbits.

A detailed, time dependent thermal analysis, including radiative heat exchange within the receiver was then formulated and used to predict the actual time variation in receiver temperature distribution and receiver outlet gas temperature throughout an orbit. Various combinations of sun-shade periods which could be encountered in near Earth orbit were considered.

The analysis includes the effect of using the heat rejection doors for temperature control of the receiver. For the purpose of this analysis a method of heat rejection door control was chosen in which they were opened or closed based on the maximum LiF temperature.

DESCRIPTION OF THE SOLAR HEAT RECEIVER

The solar receiver-collector combination is shown in figure 1. The working gas flows from the receiver inlet header to the outlet header through 48 tubes arranged circumferentially around the receiver cavity. Each gas tube is surrounded by LiF which is contained between the gas tube and an outer bellows shaped tube (containing 37 convolutions) as shown in figure 2.

The solar energy is directed through the fixed aperture by the collector and is incident on the surface of the bellows tubes. The V-shaped reflectors mounted behind and between the tubes are intended to increase the circumferential uniformity of the irradiation and to decrease the heat loss through the outer wall. The sections of gas tube between the inlet manifold and the first convolution and between the last convolution and the exit manifold are wrapped with dimpled-foil insulation to reduce the heat transfer to the working gas in these sections.

The LiF is included to function as a heat storage medium providing the unit with the capability of maintaining power system operation during shade periods of an orbit. The energy is stored as heat of fusion (450 Btu/lb at 1560⁰ F or 1046 J/g at 1122 K fusion temperature) of the LiF. In order to minimize the time variation of outlet gas temperature, it is desirable to assure that the LiF within each convolution never completely freezes or melts. In this way, advantage is taken of the relatively large effective heat capacity of the LiF during the phase change to minimize time variations in the gas tube wall temperature. In order to accomplish this, it is necessary to match the distributions of input energy along the tubes with the distributions of energy withdrawal when the LiF is in the two-phase condition, and it is necessary to control the physical distribution of the LiF. The match between distributions of energy input and withdrawal can be approached by the proper choice of receiver and collector geometries, radiative surface properties, working gas flow rate and heat transfer characteristics, the lengths of sunshade periods, and the control of the heat rejection doors. The receiver was designed in this manner with sufficient storage capacity to operate in a 60-minute sun, 38-minute shade cyclic condition. When the sun period is longer and/or the shade period is shorter, less energy storage is required and the use of the heat rejection doors (see fig. 1(b)) may be necessary to control receiver maximum temperatures. Since the LiF expands during heating, the maximum temperature must be controlled to avoid overexpansion of the LiF in the bellows tubes. The tubes were filled at 1750⁰ F (1230 K) (see

ref. 3) so the maximum LiF temperature during operation should be kept below that value. It may be desirable to use the heat rejection doors to limit the maximum LiF temperature to a level lower than the 1750^o F (1230 K) maximum allowable level in order to minimize the variations in outlet gas temperature during an orbit. The doors would be opened toward the end of a sun period if all the LiF melted and temperatures became too high and would be closed upon entering the shade period.

The control of the physical location of the LiF is made difficult by the fact that it contracts about 30 percent when it freezes. The desired distribution is maintained by the convoluted geometry of the outer tube both in zero-g and 1-g operation. The volume within the bellows tube is such that the product of the LiF mass and heat of fusion at each location along a tube exceeds by about 10 percent the required energy storage capacity at that location for the design parameters of table I.

ANALYSIS OF INSULATION REQUIREMENTS

Conservation Equations

In order to determine the maximum tolerable insulation losses as a function of orbital illumination conditions, a heat balance must be performed on the total receiver during an orbit. During a sun period, the difference between the solar input energy \dot{Q}_S , and the sum of heat transferred to the working fluid \dot{Q}_G , and the heat losses \dot{Q}_L , is equal to the energy stored in the LiF. (Symbols are defined in appendix A.)

$$Q_{ST} = \int_{\Delta t_{sun}} [\dot{Q}_S(t) - \dot{Q}_G(t) - \dot{Q}_L(t)] dt \quad (1)$$

In the general situation each of the terms in equation (1) are a function of time. For cyclic equilibrium operation, the energy stored during a sun period equals the energy withdrawn from the receiver during the following shade period; that is,

$$\int_{\Delta t_{sun}} [\dot{Q}_S(t) - \dot{Q}_G(t) - \dot{Q}_L(t)] dt = \int_{\Delta t_{sd}} [\dot{Q}_G(t) + \dot{Q}_L(t)] dt \quad (2)$$

The solar energy input term of equation (2) is a function of receiver and collector geometry; of receiver and collector radiative surface properties; of receiver-collector orientation with respect to the sun and with respect to each other; and of solar constant and solar collimation angle. The computer program developed by Schrenk and described

in reference 5 was used to calculate this quantity. For the geometry in figure 1 and for perfect orientation in a close Earth orbit, the total solar input was calculated to be 78 kilowatts.

The heat loss term in equation (2) consists of loss of radiative energy through the aperture and energy losses through the insulated surfaces of the receiver; that is,

$$\dot{Q}_L(t) = \int_A \left\{ \mathcal{F}_A [\sigma T(\bar{s}, t)^4 - \sigma T_\infty^4] + q_I(\bar{s}, t) \right\} d\bar{s} \quad (3)$$

where the integration is carried out over all of the receiver inside surface and \mathcal{F}_A represents the total radiation view factor from the point at location \bar{s} to the aperture. It should be pointed out that these factors are dependent on the effective aperture size and location, which can be changed in time by opening the heat rejection doors. The insulation heat loss is dependent on local insulation properties and temperature difference across the insulation.

The required heat transfer to the working gas is determined by the Brayton cycle desired operating points which the receiver is required to meet

$$\dot{Q}_G(t) = WC_{pG} (T_{G_{out}} - T_{G_{in}}) \quad (4)$$

where $T_{G_{out}}$ and $T_{G_{in}}$ are the specified gas temperatures at exit and inlet to the receiver. The heat transferred to the gas can also be expressed as

$$\dot{Q}_G(t) = \sum_{i=1}^{48} \int_0^L h\pi D [T_w(x) - T_G(x)] dx \quad (5)$$

where the summation is over all gas tubes and the integration is carried out along the length of each tube. Equations (4) and (5) can be used to yield the gas tube size and temperature and gas side conductance necessary to meet the design requirements of the receiver. The gas tube wall temperature appearing in equation (5) is related to the surface temperatures of the receiver cavity appearing in equation (3) which are in turn dependent on solar input and cycle times through equation (2). Detailed consideration of the heat transfer through the LiF could in principle relate the gas tube wall temperature to the cavity surface temperatures. This would, however, be extremely difficult because of the bellows geometry and because of the probable presence of both liquid and solid LiF and of voids due to the 30 percent contraction of LiF at freezing. Equations (2) to (5) are not rigorously usable without knowledge of the temperature distribution appearing in them or without the additional means of determining these temperatures.

These equations alone are not sufficient to determine these temperatures. This would require a time dependent local heat balance at each point within the receiver. Such an analysis is considered in a later section of this report. At this point, however, some useful approximations will be considered which allow use of equation (2) to estimate the maximum tolerable insulation losses as a function of sun-shade cycle times. This approach was also used in the receiver design.

Isothermal Heat Balance

In order to minimize variation in the receiver and the outlet gas temperatures, the independent parameters including geometry should be chosen so as to keep the LiF in each convolution in the two-phase condition. As long as the phase change is occurring within each convolution, the exterior surface of the bellows and the gas tube wall temperature is expected to be near the 1560° F (1122 K) LiF phase change temperature. In order then to use equation (2) to obtain a gross estimate of the potential performance, it is reasonable to assume that the LiF in each convolution always remains in a two-phase condition and that the temperature variations through the LiF can be neglected. This leads to the assumption that the surface temperatures appearing in equations (3) and (5) are 1560° F (1122 K) independent of time. Under these conditions and with the assumption that the position of the heat rejection doors is not changed with time, equation (2) can be rewritten as

$$(\dot{Q}_s - \dot{Q}_G - \dot{Q}_L)\Delta t_{\text{sun}} = (\dot{Q}_G + \dot{Q}_L)\Delta t_{\text{sd}} \quad (6)$$

If it is assumed that the gas side conductance used is a mean value, independent of time, the expression for heat transfer to the gas can be written as

$$\dot{Q}_G = 48\pi Dh \frac{[T_w - T_G(o)](1 - e^{-\beta L})}{\beta} \quad (7)$$

where

$$\beta = \frac{48\pi Dh}{WC_{pG}}$$

Since the gas flow rate, inlet and outlet temperatures are specified by the Brayton cycle design points, \dot{Q}_G is also specified and equation (7) yields the required gas side

conductance necessary to meet the design requirements when the tube surface temperature is held constant.

The loss term appearing in equation (6) consists of radiative losses through the aperture \dot{Q}_A , and of losses through the insulation \dot{Q}_I . Using the previously made assumption that the surface temperature of the bellows tubes is uniform and independent of time, an effective cavity temperature can easily be calculated so that the radiative losses through the aperture can be written

$$\dot{Q}_A = A_o \left(\sigma T_{cav}^4 - \sigma T_{\infty}^4 \right) \quad (8)$$

It will further be assumed that T_{cav} is 1560° F (1122 K) the melting point of LiF.

The value of \dot{Q}_G specified by the Brayton cycle requirements is $\dot{Q}_G = 40.5$ kilowatts. For the geometry indicated in figure 1 and for a collector efficiency of 0.9, $\dot{Q}_s = 78.0$ kilowatts. Using the assumption of equation (8) gives $\dot{Q}_A = 2.975$ kilowatts.

With these values, equation (6) was solved using \dot{Q}_I as a parameter. The results are shown in figure 3. For a given orbit period t_p , figure 3 gives the maximum tolerable insulation loss \dot{Q}_I as a function of the sun-shade times within the isothermal assumption. If for a given orbit, the actual insulation loss is greater than that given in figure 3 part of the LiF will fall below 1560° F (1122 K) during the shade period resulting in a corresponding decrease in outlet gas temperature.

As shown in the figure, a limit is imposed by the LiF storage capacity available in the receiver. The storage capacity is defined as the product of total LiF mass and the heat of fusion of LiF. If the assumed isothermal condition is to be attained, the energy stored during one cycle cannot be allowed to exceed the LiF storage capacity.

ORBITAL ILLUMINATION CONDITIONS

The actual sun-shade times encountered during an orbit depend on the orbit altitude and eccentricity and on the angle between the orbit plane and the ecliptic. For a given circular orbit, the maximum shade time occurs when the intersection of the orbital plane and the ecliptic plane coincides with the Earth-Sun line. In figure 4 the sun-shade times are given as a function of altitude for these maximum shade time conditions. Considering circular orbits for a given altitude there is a critical value of orbit inclination above which a satellite would encounter some orbits of continuous sun time during a year. The illumination conditions of several orbits are summarized in table II. Figure 4 and table II show that a large range of close Earth circular orbits have a maximum shade time of less than 38 minutes, which is the maximum shade time capability of the receiver.

The maximum shade times given in figure 4 and table II occur during relatively few days per year. As an example, the actual shade time per orbit as a function of days since launch for a 300-nautical-mile (556-km) circular orbit are given in figure 5 for three inclinations. Although the receiver must be designed and insulated to operate under maximum shade conditions, these conditions are encountered only during a small percentage of orbits per year. During most orbits, the required energy for a shade period is less than the maximum. During many of these orbits, it may become necessary to use the heat rejection doors to reject some of the excess solar energy so that the receiver temperatures and the outlet gas temperature are kept at acceptable levels in the sun period.

ORBITAL THERMAL ANALYSIS

To minimize variations of the temperatures within the receiver and of the working gas outlet temperature, it is desirable to maintain all of the LiF in the two-phase condition. This will occur only if the net solar input distribution to the bellows tubes matches the sum of the distributions along the tubes of losses and heat transfer to the gas for the uniform 1560° F (1122 K) condition. The receiver-collector geometry was chosen to approach this condition for the nominal 60-minute sun, 36-minute shade orbit. Figure 6 shows these distributions for these conditions. The curve labeled net flux input to the LiF was calculated using the analysis to be described in this section. Losses of radiative energy through the aperture and insulation losses have been deducted from these distributions. It is seen that in the central portion of the tube length, the net input exceeds the output to the gas for the 1560° F (1122 K) uniform temperature assumption. As a result, this portion of the tube can be expected to exceed 1560° F (1122 K), the LiF melting completely, during part of an orbit. For a nonuniform temperature distribution of the bellows tubes, the net input distribution curve will be modified by radiation exchange within the receiver cavity.

The distributions shown in figure 6 will, of course, change with a change in Brayton cycle operating conditions, with changes in collector and/or receiver surface conditions, with variations in receiver-collector orientation, or with changes in orbit illumination conditions. Any of these changes will then affect the local heat balance within the receiver and result in a time variation in the outlet gas temperature as local complete melting or freezing of LiF occurs. Figures 4 and 5 indicate that the orbital illumination conditions will vary in time. This together with the fact that the input and output energy distributions are not exactly matched, as shown in figure 6, indicates that the receiver will not operate with the LiF in all convolutions of the bellows tubes in the two-phase condition. The outlet gas temperature will then vary in time.

The overall heat balance based on equation (2) will not yield information concerning temperature distributions. In order to determine the time dependent receiver outlet gas temperature, it is necessary to determine the gas tube temperature distribution. Such an analysis will be presented in this section.

Thermal Model

For the thermal model on which this analysis is based, the solar receiver is divided into finite elements or nodes, each of which is assumed to be at a uniform but time dependent temperature. The model is an axisymmetric one, each node extending 360° around the receiver axis. Since the solar input flux distribution would vary in the direction around the receiver axis if the receiver-collector axis is not aligned with the solar-collector line, this analysis cannot include such a situation. The solar flux directly incident on each node was determined from distributions obtained using a computer code developed for the purpose by Schrenk (see ref. 5). Calculations made using this computer code indicated that the total solar input decreases 10 percent when the receiver-collector axis is 0.5° misoriented from the sun-collector line and decreases by 40 percent when the misorientation is 1.0° . The misorientation angle must, therefore, be held at a small value and under these circumstances the use of an axisymmetric thermal model is reasonable for the present purpose. The thermal model is shown in figure 7.

Comparison with figure 1 shows that nodes 1 to 12 correspond to the bellows tube. Node 19 simulates the heat rejection doors and node 20 corresponds to the aperture. Each of the nodes shown exchanges energy by radiation with each of the others. The total radiation view factors are calculated assuming that each node extends 360° around the receiver axis. The solar flux distribution resulting from the Schrenk computer code is shown in figure 8. This distribution is used to determine the solar energy directly incident on each node. The resulting step model is also shown in figure 8. The step model is used to calculate the net solar input to each of the nodes. All reflections are included by use of the total radiation view factors. It should be noted that nodes 13 and 16 do not represent physical surfaces but are effective surfaces (representing the regions of the inlet and outlet manifolds) used for the radiation interchange calculations. The effective absorptivity of node 19 representing the heat rejection doors is a function of the opening angle of the doors. This relation is determined as shown in appendix B.

Nodes 1 to 11 each include the thermal capacity of the LiF of three convolutions of the bellows tube, and node 12 includes the last four convolutions. Because of the complex geometry, the possible presence of two phases of LiF and a considerable void volume, and finally of the radiation boundary condition imposed on the outer surface of the bellows tube, a complete analysis of the heat transfer process through the LiF in a transient thermal analysis of the entire receiver is not tractable. For this reason, it is

assumed that the LiF can be simulated in the thermal model by only one node in the radial direction between the gas tube and the outer convoluted tube.

Time dependent, local heat balances on these LiF nodes determine the percentage of liquid and solid LiF. When an individual node either completely melts or freezes, its temperature changes. As a result, the gas tube wall temperature and hence the gas temperature is changed.

Even if the LiF in all convolutions always remained in the two-phase condition, the receiver outlet gas temperature would still be expected to vary in time. Since the percent of solid LiF and hence the position of the 1560° F (1122 K) solid-liquid interface would vary continuously in each convolution, and since the void volume would vary in size and position, the resistance to heat transfer through the LiF would continuously vary. This together with the fact that the outer surface temperatures of the convoluted tubes would vary due to the changes in irradiation from the sun period to the shade, would result in a time variation in the gas tube wall temperature and hence in gas temperature. The variations in the gas tube wall temperature while the LiF phase change is occurring will, however, be much smaller than those occurring when only one phase of LiF is present because of the large difference in the effective thermal mass.

Because of the lack of knowledge of the effective thermal conductivity of the LiF in this geometry with the presence of voids and two phases, the resistance to heat transfer through the LiF is not included in this analysis. As a result, the analysis does not predict the gas temperature variations which can be attributed to variations in LiF thermal resistance, but it does show the much larger effects of complete melting or freezing of the LiF in any node.

The neglect of thermal resistance of the LiF and the use of only one LiF node radially from gas tube to the outer tube leads to the additional assumption that the temperatures of the outer convoluted tube and the gas tube are equal to that of the LiF adjacent to them. Finally, since the LiF thermal resistance is neglected and since reflectors are positioned behind and between the tubes to increase the uniformity of their irradiation, circumferential temperature gradients around individual tubes are neglected.

Conduction between the nodes of the top and aperture cones is not included. The temperature of these metal surfaces is largely determined by the radiative flux incident on them and this effect is included. Since conduction in the LiF is not included, this additional assumption of neglecting it elsewhere is reasonable. Neglecting conduction throughout the receiver is a considerable savings in computational effort while the major thermal characteristics of the receiver are retained.

The gas tubes are wrapped with dimpled multifoil insulation in the regions between the inlet manifold and the first convolution of the bellows tube and between the last convolution and the exit manifold to minimize the heat transfer to the gas in these regions. In the thermal model, nodes 13 and 16 represent these regions. Heat transfer to the gas is assumed not to occur from these nodes but only from nodes 1 to 12. The LiF nodes

are coupled through their energy exchange with the gas flow as well as through radiative exchange.

Another basic assumption made in the analysis is that only the thermal capacity of the LiF is important in determining the transient thermal performance of the receiver, the heat capacities of all the other materials in the receiver being neglected. This is a reasonable approximation since the heat of fusion and specific heat of the LiF will make the LiF, by far, the largest thermal mass in the system. For example, the thermal masses of the receiver are about 117 000 Btu (1.23×10^8 J) for the heat of fusion of all LiF, 160 Btu/ $^{\circ}$ F (3.04×10^5 J/K) for all LiF assuming single phase, and 75 Btu/ $^{\circ}$ F (1.42×10^5 J/K) for all other materials. It can be seen that for a temperature variation of 100° F (56 K) during an orbit, for example, with much of the LiF passing through the two-phase condition, that the thermal mass of the LiF will be much more important than other materials in determining the transient behavior of the system; that is, 7500 Btu (7.91×10^8 J) sensible heat for all other materials compared to 133 000 Btu (1.40×10^8 J) latent and sensible heat of the LiF.

Formulation

Since the thermal capacity of the LiF is the only one included in the analysis, the transient solutions are centered around the time dependent heat balance on the LiF nodes; that is,

$$\left(mC_p\right)_i \frac{dT_i}{dt} = q_{R_i} - q_{G_i} - q_{I_i} + S_i \quad W_{S_i} = 0, 1 \quad (9)$$

$$\left(m \Delta h_f\right)_i \frac{dW_{S_i}}{dt} = q_{R_i} - q_{G_i} - q_{I_i} + S_i \quad 0 < W_{S_i} < 1 \quad (10)$$

where W_{S_i} is the ratio of solid LiF mass in node i to the total LiF mass in node i .

The radiation exchange for node i is given by

$$q_{R_i} = \sum_{\substack{j=\text{all} \\ \text{surfaces}}} A_i \mathcal{F}_{ij} \left(\sigma T_j^4 - \sigma T_i^4 \right) \quad (11)$$

where the summation is taken over all surfaces making up the receiver cavity enclosure. The total view factors appearing in equation (11) are a function of the geometry of the

entire enclosure and the emissivities of all surfaces comprising the enclosure (see ref. 4). The emissivities of the nodes representing the LiF surrounded by the columbium convoluted tube can be taken as effective values to account for the convoluted geometry. The emissivity (or absorptivity) of the node representing the heat rejection doors is taken as an effective value which can be varied in time to account for movement of the doors. The relation between the effective absorptivity and the door position is developed in appendix B. The temperatures of the LiF nodes which appear in equation (11) at each time increment are obtained from solution of equations (9) and (10). The temperature of the aperture node (and of the heat rejection door node when they are open) is taken as T_∞ , the effective sink temperature. The temperatures of all the other nodes, which do not consist of LiF, can easily be obtained at each increment in time since the capacities of these nodes and the conductive heat transfer to these nodes has been neglected. Equating the energy input and loss for each yields the following expression for the temperature of each such node:

$$\sigma T_i^4 = \frac{S_i + \sum_{j=\text{all surfaces}} A_j \mathcal{F}_{ji} \sigma T_j^4 - q_{I_i}}{\epsilon_i A_i} \quad (12)$$

where the summation is again over all surfaces making up the receiver cavity enclosure. The insulation loss term in equation (9) is assumed for convenience to be given by

$$q_{I_i} = \left(\frac{A_i}{\sum_j A_j} \right) \dot{Q}_I \quad (13)$$

where the summation is over all nodes excluding the aperture and \dot{Q}_I is the specified insulation loss from the entire receiver. Of course, the distribution assumed in equation (13) is arbitrary and can be easily changed depending on the actual insulation system used.

The heat transfer to the gas from node i depends on the local gas temperature which, in turn, depends on the temperatures of all the upstream nodes. The axial distribution of the bulk mean gas temperature for one-dimensional flow is given by

$$WC_{pG} \frac{dT_G}{dx} = q'_G \quad (14)$$

where

$$q'_G = hN\pi D [T_w - T_G(x)] \quad (15)$$

The thermal inertia of the gas has been neglected in equation (14). This is the quasi-steady approach which assumes that the time rate of change of T_w is much less than that of T_G and is accurate for this situation. The solution of equations (14) and (15) for a constant wall temperature is

$$T_G(x) = T_w - [T_w - T_G(0)] e^{-\beta x} \quad (16)$$

where T_w and β are constants and where

$$\beta = \frac{hN\pi D}{WC_{pG}}$$

Substitution of equation (16) into equation (15) yields

$$q'_G = hN\pi D [T_w - T_G(0)] e^{-\beta x} \quad (17)$$

Integrating this over a flow length L yields

$$\int_0^L q'_G dx = \frac{hN\pi D [T_w - T_G(0)]}{\beta} (1 - e^{-\beta L}) \quad (18)$$

Equations (16) and (18) can be used to give the gas temperature and heat transfer to the gas in the present situation where it has already been assumed that h or β is constant and the gas tube wall consists of a series of constant temperature finite length LiF nodes. Let x be measured in the direction of the flow and x_i be the distance from the beginning of the heated flow length to the downstream end of node i . Then the temperature of the gas at the downstream end of node i can be written from equation (16) as

$$T_{G_i} \equiv T_G(x_i) = T_i - (T_i - T_{G_{i-1}}) e^{-\beta(x_i - x_{i-1})} \quad (19)$$

Then the heat transferred from node i to the gas flow can be written from equation (18) as

$$q_{G_i} = \frac{hN\pi D}{\beta} (T_i - T_{G_{i-1}}) \left[1 - e^{-\beta(x_i - x_{i-1})} \right] \quad (20)$$

This is a convenient method of calculating the heat transfer to the gas because it has the unique advantage of yielding the correct receiver outlet gas temperature when all the LiF is at the 1560° F (1122 K) phase change temperature without the additional complications and error involved in treating the gas flow as finite nodes.

The solar input term S_i in equation (9) is the net solar input to node i at time t . It is given by

$$S_i = A_i \alpha_i \Psi_i + A_i \sum_{\substack{j=\text{all} \\ \text{surfaces}}} \mathcal{F}_{ij}^s \Psi_j \frac{1 - \alpha_j}{\alpha_j} \quad (21)$$

where the summation is over all surfaces of the receiver cavity. The term Ψ_i is the solar flux directly incident on node i and is obtained using the computer code developed by Schrenk and is given in figure 8. If a node is not directly illuminated by solar radiation, the Ψ_i value is zero. During the shade period of the orbit, all the Ψ values are set equal to zero. The total radiation view factors appearing in equation (21) are obtained using absorptivities for solar radiation. The superscript s is used to distinguish them from those appearing in equation (11).

Solution Procedure

The conditions of the LiF nodes are determined by integrating equations (9) and (10) with respect to time for all LiF nodes simultaneously. Equation (9) is used for a particular node to determine its temperature when it is single phase. The specific heat appearing in this equation is either the value for liquid or solid LiF. Equation (10) is integrated for each node when it is in the two-phase condition. The terms on the right sides of equations (9) and (10) are evaluated using equations (11) to (13), (20), and (21). In order to solve equation (11) for each LiF node, it is necessary to simultaneously determine the temperatures of all nodes other than the LiF nodes and the aperture using equation (12).

With the receiver temperatures known at any point in time, the temperature profile and exit temperature of the gas is determined using equation (19). The heat rejection door operation is simulated by changing the effective emissivity of the node representing them. This changes the \mathcal{F} factors appearing in equations (11) and (21). For purposes of this analysis the heat rejection door position is controlled by the maximum LiF temperature. It is assumed that the doors begin opening at a constant rate (assumed $20^\circ/\text{min}$ for this analysis) when the hottest LiF node reaches some specified temperature designated T_{DO} and continue to open until that node again falls below T_{DO} . It is assumed that they remain open at this position until the hottest LiF node falls below another specified temperature designated T_{DC} when they begin closing (which continues until fully closed or until the hottest LiF node again reaches T_{DO}). The heat rejection doors are always in the closed position during a shade period. The temperature T_{DO} should be specified below 1750° F (1230 K) the temperature at which the LiF would be overexpanded within the bellows tubes.

The emissivity of the LiF nodes is taken as an effective value to account for the bellows geometry of the tubes. Since the bellows tubes are closely spaced around the circumference of the receiver, the effective wall of the cavity appears to approximate a surface which has continuous circumferential grooves. This fact was used to estimate the effective emissivity using the values for rectangular grooves (see ref. 4) and the results are given in figure 9. The spread of values indicated results from the variation of convolution depth along the tubes. The bellows tubes in the receiver are grit-blasted Cb-1 percent Zr with an emissivity at these temperatures ranging from 0.30 to 0.45 and a solar absorptivity from 0.60 to 0.67. Using figure 9 it is seen that this results in an effective emissivity of the LiF nodes ranging from 0.40 to 0.60 and a solar absorptivity from 0.70 to 0.77.

The value of the gas side conductance used in the analysis was $h = 15.16 \text{ Btu}/(\text{hr})(\text{ft}^2)(^\circ\text{F})$ or $86.1 \text{ W}/(\text{m}^2)(\text{K})$. This is the value which yields the design performance shown in table I for the heat transfer length of the receiver and a uniform gas tube temperature at the 1560° F (1122 K) phase change temperature. The receiver gas tubes are ring-dimpled in order to attain this value. The value has been confirmed by experiment.

RESULTS AND DISCUSSION

A Fortran IV computer program was written to solve equations (9) to (21) according to the outlined procedure. This program was used to predict the receiver thermal performance during Earth orbit. The effects of receiver insulation losses, of bellows tube emissivity and solar absorptivity, of heat rejection door operation, and of length of shade period are illustrated for the present receiver design by the results presented in

this section. The method of heat rejection door control assumed for this analysis was explained in the previous section.

As indicated by figure 3 there is a minimum insulation required for satisfactory receiver performance for each orbit considered. For a 60-minute sun, 36-minute shade orbit, which approximates the worst illumination conditions for a 300-nautical-mile (556-km) circular orbit, the maximum tolerable total insulation loss given by figure 3 is about 5 kilowatts. If more than this minimum insulation would be used, the receiver would operate at higher temperatures. The equilibrium cyclic conditions obtained by use of the computer program described are given in figures 10 and 11 for values of \dot{Q}_I of 3 and 5 kilowatts. In figure 10, the outlet gas temperature and temperature of the hottest node (node 2 in this case) are plotted for one orbit. The first 36 minutes constitute the shade period. In figure 11, the condition of the LiF along the tube is shown at several points during the orbit. For both cases most of the LiF nodes are melted and heated above 1560°F (1122 K) at the end of the sun period and the first LiF node is completely frozen at the end of the shade period. These effects are seen to be reflected in the outlet gas temperature shown in figure 10.

The results for the $\dot{Q}_I = 3$ kilowatts case in figures 10 and 11, show the effect of the use of the heat rejection doors at the end of the sun period. For the cases in figures 10 and 11 T_{DO} (the temperature of the hottest LiF node at which the heat rejection doors begin to open) was 1680°F (1189 K). The hottest node in this situation was node 2. As shown, it reached 1680°F (1189 K) about 4.5 minutes before the end of the sun period and reached a peak value of only a few degrees above 1680°F (1189 K). The door opening reached 20° before this maximum LiF temperature fell below 1680°F (1189 K). This position was held until the end of the sun period at which time the heat rejection doors were closed. Had the maximum LiF temperature fallen below 1650°F (1172 K) (the value taken for T_{DC} , the temperature of the hottest LiF at which the heat rejection doors begin to close) before the end of the sun period, the doors would have begun closing. For the higher insulation loss case the LiF did not reach the temperature level which was set to initiate heat rejection door operation.

The effects on performance of changing the solar absorptivity and emissivity of the bellows tubes are shown in figures 12 to 15. In figures 12 and 13 a comparison is made between the effects of an emissivity of 0.40 and 0.90. The higher value would correspond to the use of an emissive coating, the lower to a typical value for the grit-blasted surface used. It is desirable to keep the receiver at as nearly a uniform temperature as possible. Figure 12 shows that, for a wide range of emissivities the effect on receiver performance, as measured by outlet gas temperature, is rather small. The higher emissivity does result in a more uniform temperature profile along the tubes as shown in figure 13 but the difference between the two results is not large considering the large difference in the two values of emissivity. Since the incident solar flux is high and since its variation along the tubes is so marked, a change in solar absorptivity which

would in turn change the net solar input distribution, would be expected to make an appreciable difference in the receiver thermal conditions. In figure 14, it is seen that the outlet gas temperature, for these conditions, does not vary significantly for the range of effective absorptivities which could be obtained with grit-blasted bellows tubes. However, the temperature distributions along the tubes are significantly different for this relatively small variation in absorptivity. In figure 14, the time variation of the hottest node is plotted for each case. As indicated, the location of the hottest node moves along the tube as absorptivity is decreased. Of the three cases considered, a value of $\alpha_E = 0.65$ results in the most uniform temperature profile. Values of absorptivity lower than this would result in the exit end LiF being heated to significantly higher temperatures than that along the rest of the tube. The receiver performance is much more sensitive to changes in absorptivity than in emissivity. The distribution of net solar energy input is more significant in determining the receiver thermal conditions than is thermal radiative exchange within the cavity. Since the net distribution of solar input is dependent on receiver-collector geometry and orientation, and collector surface conditions as well as receiver surface absorptivity, the optimum solar absorptivity would change with any variation in these other factors.

As shown in figure 5, the shade time per orbit for a 300-nautical-mile (556-km) circular orbit varies considerably during a year. The worst illumination conditions of about 60-minute sun and 36-minute shade periods were considered in figures 10 to 15. During days in which the shade period is less than this, it becomes necessary to open the heat rejection doors for a period during every orbit. The cyclic equilibrium conditions for several such cases are given in figures 16 to 19. Obviously, the shorter the shade period, the higher the energy storage remaining at the end of the shade period and the less the requirements of total energy input during the sun period. In figure 16, the shorter the shade period, the sooner the outlet gas temperature rises above 1500°F (1089 K) during the sun period and the sooner the hottest node reaches the temperature at which the heat rejection doors begin to open. In the 32-minute shade period case of figure 16, the heat rejection doors began opening 57 minutes into the sun period and reached an opening angle of 20° . In the 28-minute shade case they began opening 50 minutes into the sun period and reached an opening angle of 15° . In both cases the sun period ended before the hottest LiF node cooled sufficiently to begin closing the heat rejection doors. The profiles in figure 17 show that the temperatures are more uniform at the end of the sun period for the shorter shade periods. As expected, the energy storage, as indicated by the percent solid LiF, is higher for the shorter period considered in figure 17. The results shown in these figures are obviously dependent on the means chosen to control the heat rejection door position. The 30°F (17 K) spread between T_{DO} and T_{DC} , the temperatures at which heat rejection door movement is initiated, results in appreciable variations in the outlet gas temperature. A continuous sun case is included in figure 16 to illustrate this further. The temperature plot of the

hottest node shows that it continuously varies between temperature T_{DO} and T_{DC} , the heat rejection doors moving between 10° and 15° opening angles. This then results in a variation of over 30° F (17 K) in outlet gas temperature.

One approach which might be taken to reduce these gas temperature variations and to lower the highest temperature level which the gas reaches is to open the heat rejection doors sooner and control them more closely. In figure 18 these same sun-shade combinations are shown for values of $T_{DO} = 1650^\circ$ F (1172 K) and $T_{DC} = 1640^\circ$ F (1167 K). As indicated in the plot of hottest node temperatures, the doors open and close tending to keep the hottest LiF between the temperatures T_{DO} and T_{DC} . As in figure 17, the temperature profile in figure 19 shows that the shorter shade period results in more uniform temperatures. Figure 19, however, shows that in this case the last several LiF nodes along the tube completely freeze during the shade period for the worst illumination case of 60-minute sun and 36-minute shade. This results in the significant drop in outlet gas temperature at the end of the shade period shown for this case in figure 18. This all results from the fact that, for $T_{DO} = 1650^\circ$ F (1172 K), the heat rejection doors are opened for about 2 minutes at the end of the sun period. During this time, enough energy is lost to keep the hottest LiF node below 1650° F (1172 K) but enough energy is also lost from the downstream nodes so that the stored energy and radiative exchange is insufficient to meet the requirements during the following shade period. To avoid an unnecessary gas temperature drop at the end of the shade periods, the energy storage must be increased in these downstream nodes. For the present design this can be done by raising T_{DO} and T_{DC} and therefore reducing the amount of energy they lose through the heat rejection doors or by increasing the solar input to these nodes during the sun period. One effective way of accomplishing the latter is to lower the solar absorptivity as already shown in figures 14 and 15. Lowering it from 0.75 to 0.70 is sufficient to avoid freezing the downstream LiF as shown in figures 20 and 21 where both cases are plotted for comparison. As previously stated, both these values of absorptivity are within the range which can be achieved with grit-blasted bellows tubes. The results in figures 18 to 21 demonstrate that the variation in outlet gas temperature can be held within the acceptable range of 1490° to 1550° F (1080 to 1120 K) for the present receiver design. Changes in the heat rejection door design to allow more selective heat rejection from only the hottest parts of the receiver could result in further narrowing the range of outlet gas temperature but would result in added complexity of design and control.

The heat balance per orbit for most of the cases considered in figures 16 to 19 are given in table III. As the sun period is increased and consequently the solar input per orbit is increased the heat rejected through the doors is increased to compensate. For the higher value of T_{DO} and for the shorter shade periods, figures 16 to 19 showed that the receiver temperatures were higher for longer periods of time. This is reflected in higher energy transfer to the gas and aperture losses as shown in table III. Table III

does not show a variation in insulation loss as might be expected physically because the value was specified and held constant in this analysis. The energy storage is defined as zero when all the LiF is at 1560° F (1122 K) and 100 percent solid. The values given in table III therefore are the energy difference between the actual state of the LiF and the condition defined as zero energy storage.

CONCLUDING REMARKS

A preliminary thermal performance analysis was performed for the solar receiver. A simplified overall receiver heat balance was first used to estimate the maximum tolerable insulation losses as a function of orbital illumination conditions. A digital computer analysis was then used to predict the variations in receiver outlet gas temperature and LiF conditions throughout a close Earth orbit. The thermal model used is simple enough to make the analysis tractable but retains the most important characteristics of the receiver. For purposes of this analysis a simple method was assumed for selecting the heat rejection door position by sensing the maximum LiF temperature. The thermal conditions of the receiver were examined to determine the effects of radiative surface properties, insulation losses, and shade period length.

Effective values of emissivity and solar absorptivity were used to account for the bellows geometry of the tubes. The analysis showed that the receiver performance is more sensitive to variations in solar absorptivity than in emissivity. The outlet gas temperature variation when the tubes have a high emissivity, such as could be obtained by use of a coating, was not found to differ significantly from the case where the tubes were assumed to have the lower emissivity corresponding to a grit-blasted surface. The solar absorptivity obtained using grit-blasted bellows tube surfaces is near the optimum value for the receiver-collector design considered. The effective absorptivity of the grit-blasted bellows tubes was predicted to range between 0.70 and 0.77. For one of the worst illumination conditions considered, the lower value was found to yield results with less variation in outlet gas temperature.

In all the cases considered, the outlet gas temperature showed some decrease at the end of each shade period and some increase at the end of each sun period. In most cases, the gas temperature decrease during the shade period was due solely to freezing of the LiF in the first few convolutions along the gas flow length. The net solar input to this region is insufficient to meet the local heat storage requirements. At the end of each sun period some LiF was found to be locally completely melted and superheated, resulting in the rise in outlet gas temperature. This results from the fact that the distribution of solar input never exactly matches the required heat storage distribution which would result in isothermal operation. This temperature rise near the end of the sun periods can be reduced by having the heat rejection doors partially open near the end

of sun periods, but it cannot for this design be entirely eliminated without jeopardizing the operation during the shade periods.

The amount of variation in the outlet gas temperature in time is a function of the receiver surface radiative properties, the amount of insulation losses, the relative lengths of the sun and shade periods, and the method of heat rejection door control. The results indicate that, if the insulation losses are held below the maximum allowable level calculated, the heat rejection doors can be used to hold the outlet gas temperature variation within an acceptable range of about 1490° to 1550° F (1080 to 1120 K). For 78-kilowatt solar input, corresponding to a 30-foot- (9.14-m-) diameter collector, the maximum allowable insulation loss for a 60-minute sun, 36-minute shade orbit is 5 kilowatts.

Lewis Research Center,
National Aeronautics and Space Administration,
Cleveland, Ohio, December 7, 1970,
128-70.

APPENDIX A

SYMBOLS

A	area
A_o	area of aperture
C_p	specific heat
D	diameter of gas tube
\mathcal{F}	total radiation view factor
\mathcal{F}_A	total radiation view factor to aperture
\mathcal{F}_{ij}	total radiation view factor from node i to node j
\mathcal{F}_{ij}^S	total radiation view factor from node i to node j for solar radiation
h	conductance
Δh_f	latent heat of fusion of LiF
L	heat transfer length of gas tubes
m	mass
N	number of gas tubes
\dot{Q}_A	rate of heat loss through aperture
\dot{Q}_G	rate of heat transfer to gas
\dot{Q}_I	total insulation loss
\dot{Q}_L	rate of heat loss
\dot{Q}_S	rate of solar energy input
Q_{ST}	energy stored in one orbit
q'_G	convection per unit length of gas tube
q_{G_i}	convection to node i
q_I	insulation loss flux
q_{I_i}	insulation loss from node i
q_{R_i}	radiation to node i
S_i	net solar input to node i
\bar{s}	distance

T temperature
 T_{DC} temperature of hottest node at which heat rejection doors begin to close
 T_{DO} temperature of hottest node at which heat rejection doors begin to open
 T_{∞} sink temperature
 t time
 t_p orbital period
 Δt_{sd} shade period length
 Δt_{sun} sun period length
 W mass flow rate of gas
 W_{S_i} fraction of LiF in node i which is solid
 x distance along gas tubes in flow direction
 α solar absorptivity
 β $hN\pi D/WC_{pG}$
 ϵ emissivity
 Ψ_i direct solar flux on node i

Subscripts:

E effective value
 G gas
 i refers to node i
 w gas tube wall

APPENDIX B

HEAT REJECTION DOOR EFFECTIVE ABSORPTIVITY

The hexagonal aperture cone of the receiver is approximated by a circular cone in the thermal analysis. The effective emissivity of one of the nodes which comprise this cone in the thermal model is changed as a function of time in order to simulate movement of the heat rejection doors. The relation between effective emissivity and door opening angle which was used in the analysis is developed here.

When the doors are partially open, part of the radiation incident on the doors is reflected and/or reradiated back into the receiver and part is lost to space as indicated in figure 22. For the purpose of calculating the radiation exchange within the receiver cavity and the radiative energy loss to space, the conical opening of the heat rejection doors can be assumed to have an effective temperature of zero and an effective absorptivity defined

$$\alpha_E = 1 - \frac{Q_2}{Q_1} \quad (B1)$$

where the Q 's are defined in figure 22.

It is assumed that there are six heat rejection doors, they are hinged at their upper ends, are perfectly insulated, and when closed form a continuous conical surface referred to as the heat rejection door node in the receiver thermal analysis. As the doors are opened, the effective absorptivity of the door opening is determined from equation (B1). The terms appearing in this equation are determined by considering the enclosure defined by the door opening (surface 1), the swing arc (surface 2) and the conical surface which includes the doors (surface 3). As the opening angle increases, the area of surface 3 increases. The area of the actual door surfaces, however, remains constant and is equal to the area of the opening A_1 . The difference between A_3 and A_1 is the area of the gaps formed between adjacent doors as they are opened. The geometric configuration factors between surfaces 1, 2, and 3 are calculated using the expression for the configuration factor between coaxial disks and configuration factor algebra. Then, denoting the actual door surfaces as surface 3D and the gaps as surface 3G (i. e., $A_3 = A_{3D} + A_{3G}$) the following approximations are made:

$$F_{2-3D} = \frac{A_{3D}}{A_3} F_{2-3}$$

$$F_{2-3G} = \frac{A_{3G}}{A_3} F_{2-3}$$

If these and configuration factor algebra are used, all the configuration factors between the four surfaces 1, 2, 3D, and 3G can be easily obtained. Then using an emissivity of unity for surfaces 1, 2, and 3G and the surface emissivity of the doors for surface 3D, the total configuration factors are calculated. The terms appearing in equation (B1) can then be calculated in a straightforward manner to yield

$$\alpha_E = 1 - \mathcal{F}_{1-1} - \frac{\mathcal{F}_{1-3D}\mathcal{F}_{3D-1}}{\epsilon_{3D} - \mathcal{F}_{3D-3D}} \quad (\text{B2})$$

For a value of $\epsilon_{3D} = 0.4$ (typical) the effective absorptivity of the heat rejection door node plotted against opening angle is given in figure 23.

REFERENCES

1. Brown, William J.: Brayton-B Power System - A Progress Report. Proceedings of the 4th Intersociety Energy Conversion Engineering Conference. AIChE, 1969, pp. 652-658.
2. Klann, John L.: Steady-State Analysis of a Brayton Space-Power System. NASA TN D-5673, 1970.
3. Gnadt, P. A.: Filling Heat Storage Tubes for the Solar Brayton-Cycle Heat Receiver with Lithium Fluoride. ORNL - TM-2732, Oak Ridge National Laboratory, July 1970.
4. Siegel, R.; and Howell, J. R.: Thermal Radiation Heat Transfer, Vol. 2, Radiation Exchange Between Surfaces and in Enclosures. NASA SP-164, 1969.
5. Schrenk, G. L.; and Gritton, D. G.: Analysis of Solar Reflectors. Mathematical Theory and Methodology for Simulation of Real Reflectors. Final Report, Allison Division, General Motors Corp., 1963. (Also available as DDC AD-602870.)

TABLE I. - SOLAR RECEIVER DESIGN CONDITIONS

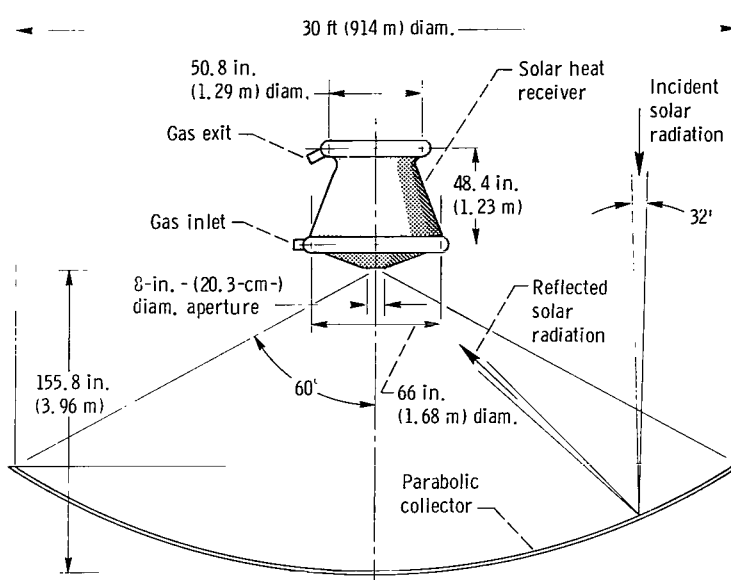
Working fluid	Helium-xenon - 83.8 mol. wt.
Gas inlet temperature, °F (K)	1098 (866)
Gas exit temperature, °F (K)	1500 (1089)
Gas flow rate, lb./sec (kg/sec)	1.607 (0.729)
Gas inlet pressure, psia (N. m ² abs)	53.9 (3.72×10 ⁵)
Gas pressure drop	2 percent of inlet pressure
Minimum time in sun, min	60
Maximum time in sun	Continuous
Maximum time in shade, min	38

TABLE II. - ORBIT ILLUMINATION CONDITIONS

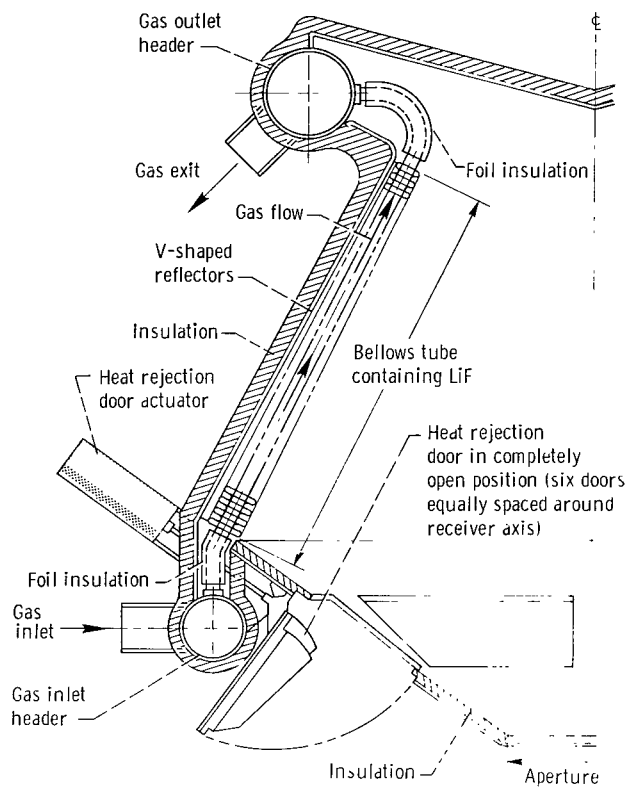
Altitude		Period, min	Maximum shade time		Minimum sun time, min	Critical inclina- tion, deg	Orbit inclination, deg			
n mi	km		min	Percent of orbit			30	60	90	
200	370	91.8	36.2	39.4	55.6	47.4	0	26	78	
300	556	95.4	35.5	37.2	59.9	43.4	↓	36	95	
500	926	103.2	34.9	33.8	68.3	37.3	↓	52	119	
700	1296	111.6	34.8	31.2	76.8	32.7	↓	76	139	
1000	1852	123.6	34.9	28.2	88.7	27.3	↓	100	160	
5000	9260	324.0	43.3	13.4	280.7	.6	↓	203	267	268

TABLE III. - HEAT BALANCE FOR 96-MINUTE ORBIT WITH SOLAR INPUT OF 78 KILOWATTS
 [Insulation loss, 8.0 kW-hr; effective solar absorptivity $\alpha_E = 0.75$; effective emissivity $\epsilon_E = 0.4$]

Case	Energy to gas. kW-hr	Loss to aperture. kW-hr	Loss through heat rejection doors. kW-hr	Energy storage. kW-hr		Solar input. kW-hr	Sun period. min	Shade period. min	Temperature of hottest node at which heat rejection doors be-		Temperature of hottest node at which heat rejection doors be-	
				Beginning of shade	Beginning of sun				gin to open.		gin to close.	
									T_{DO}		T_{DC}	
									$^{\circ}F$	K	$^{\circ}F$	K
1	65.05	4.96	0.00	34.27	5.26	78.0	60	36	1680	1189	1650	1172
2	64.62	4.76	.62	30.46	1.78	78.0	60	36	1650	1172	1640	1167
3	66.06	4.97	4.17	34.08	3.25	83.2	64	32	1680	1189	1650	1172
4	65.30	4.91	5.01	33.10	7.36	83.2	64	32	1650	1172	1640	1167
5	67.12	5.01	8.27	33.96	11.49	88.4	68	28	1680	1189	1650	1172
6	66.18	4.92	9.30	33.47	10.88	88.4	68	28	1650	1172	1640	1167



(a) Solar heat receiver, solar collector combination.



(b) Solar heat receiver cross section.

Figure 1. - Brayton solar heat receiver.

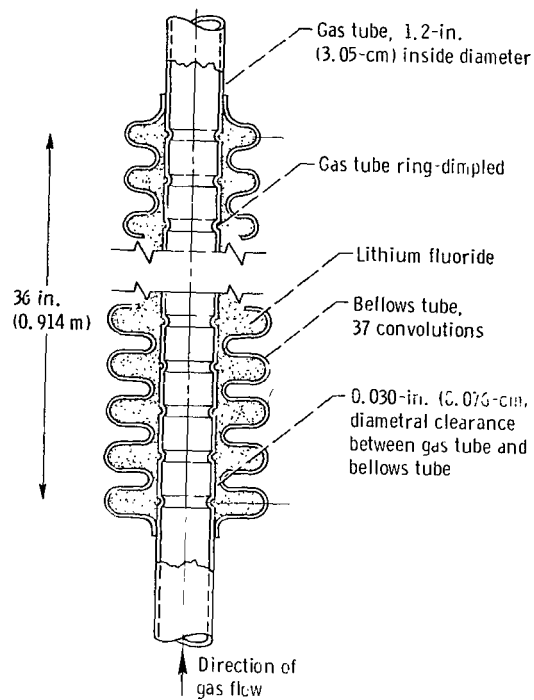


Figure 2. - Heat transfer heat storage tube.

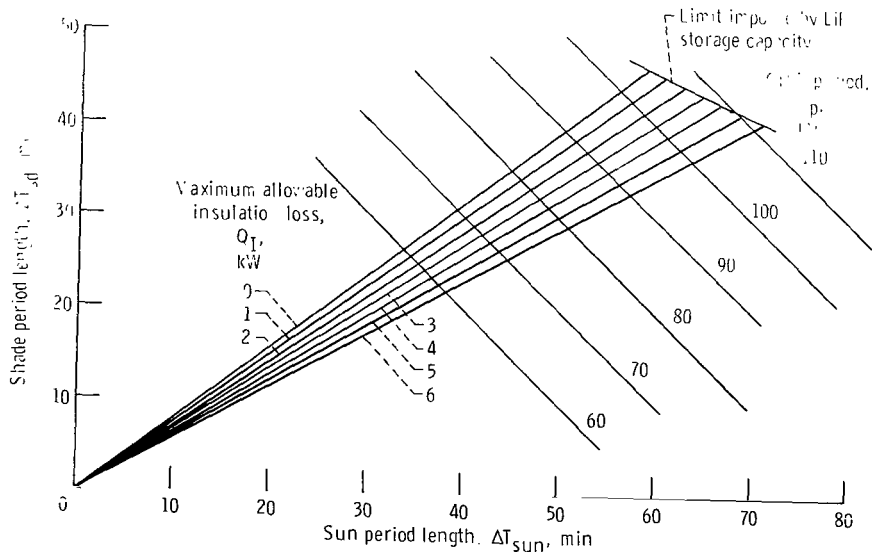


Figure 3. - Maximum allowable insulation loss.

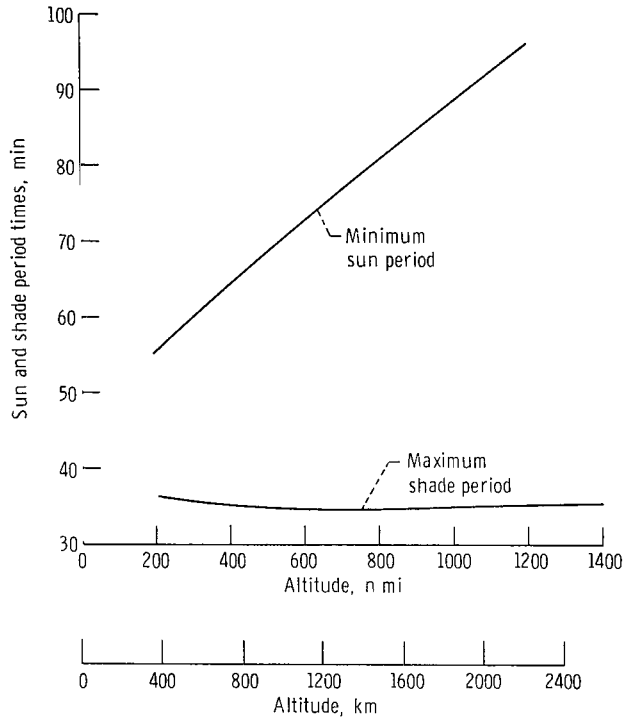


Figure 4. - Minimum sun and maximum shade periods plotted against altitude for circular Earth orbits.

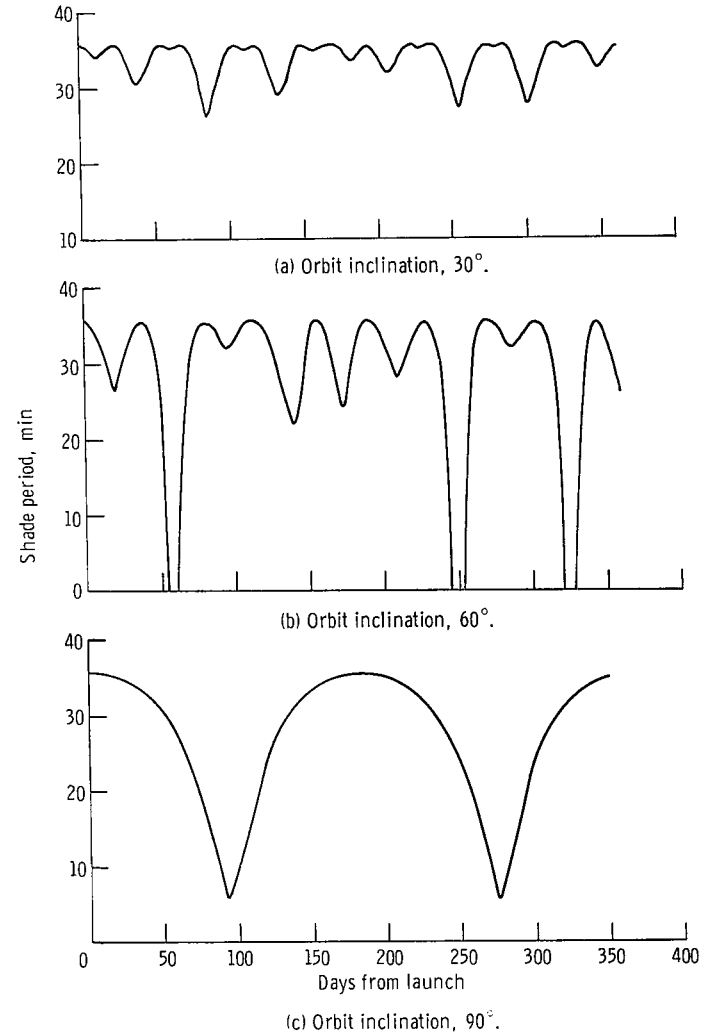


Figure 5. - Shade period per orbit for 300-nautical-mile (556-km) circular orbit.

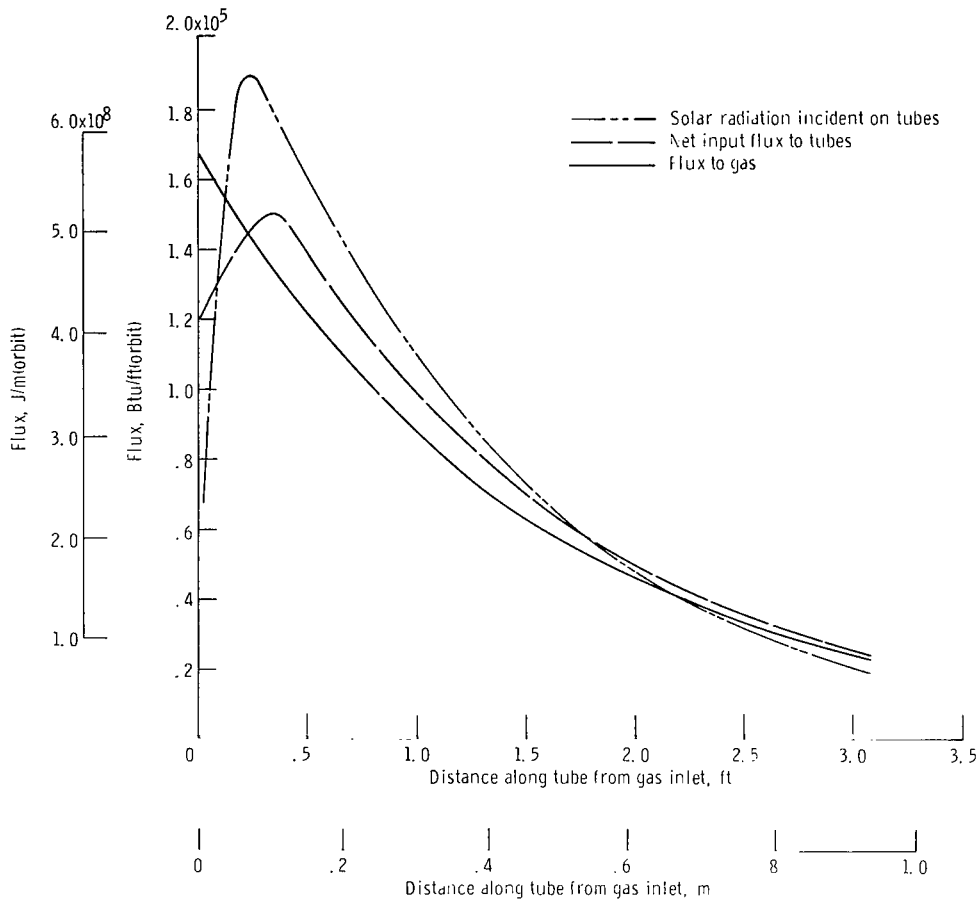


Figure 6. - Flux distributions along gas tube length for 60 minute sun period, 36-minute shade period orbit.

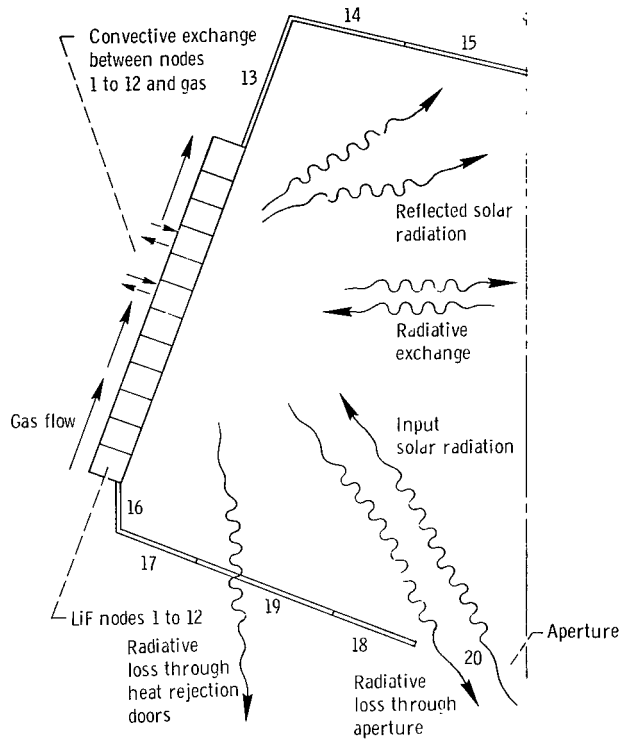


Figure 7. - Nodal model for orbital thermal analysis.

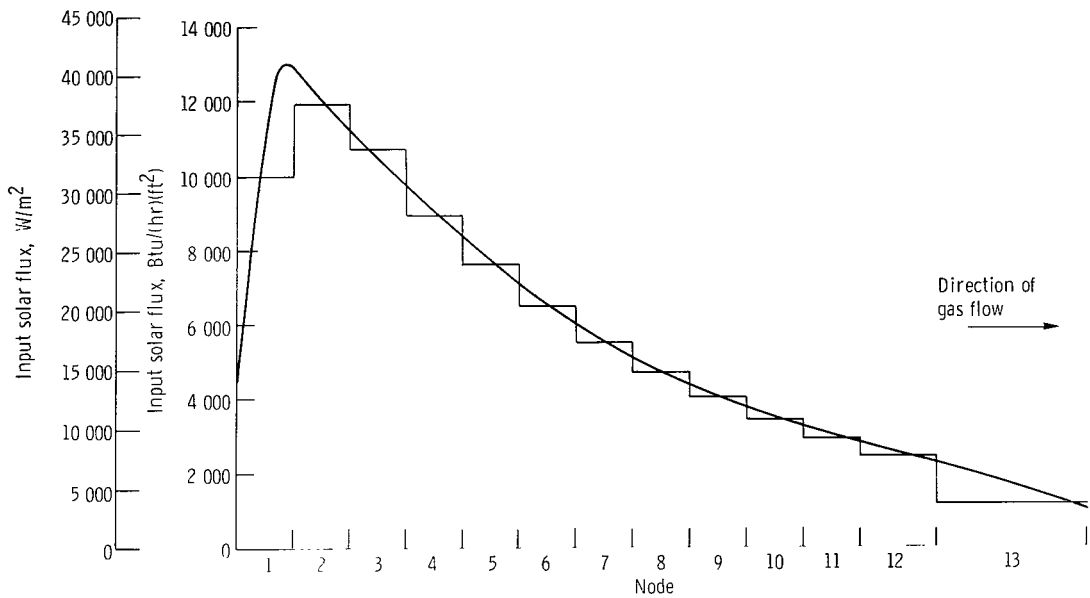


Figure 8. - Input solar flux distribution.

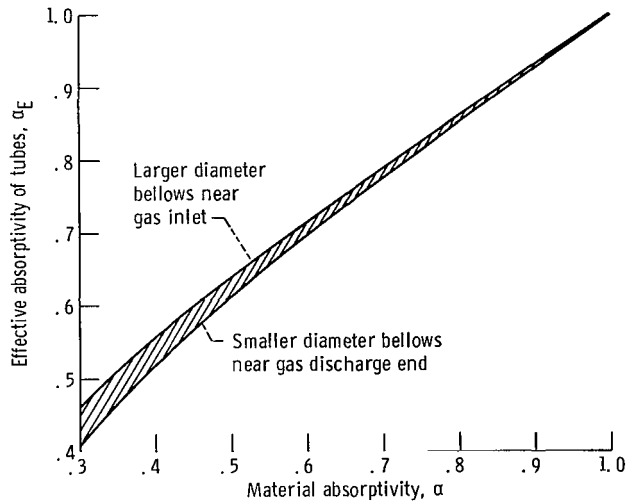


Figure 9. - Estimate of effective absorptivity of bellows tubes in receiver cavity.

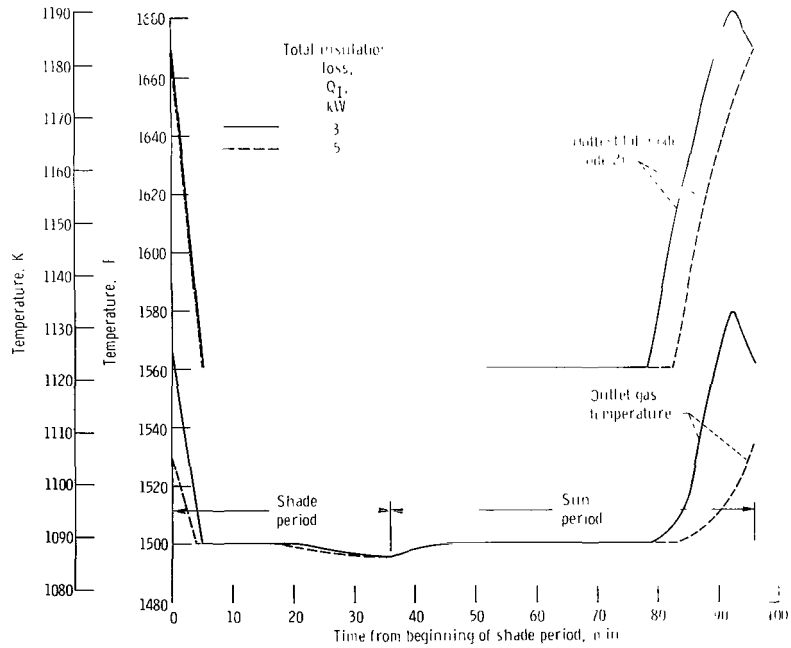


Figure 10. - Performance for 60-minute sun, 36 minute shade period orbit. Temperature of hottest node at which heat rejection doors begin to open, 1680 F (1199 K); temperature of hottest node at which heat rejection doors begin to close, 1650 F (1172 K); bellows tube surface effective emissivity, 0.4; effective solar absorptivity, 0.75.

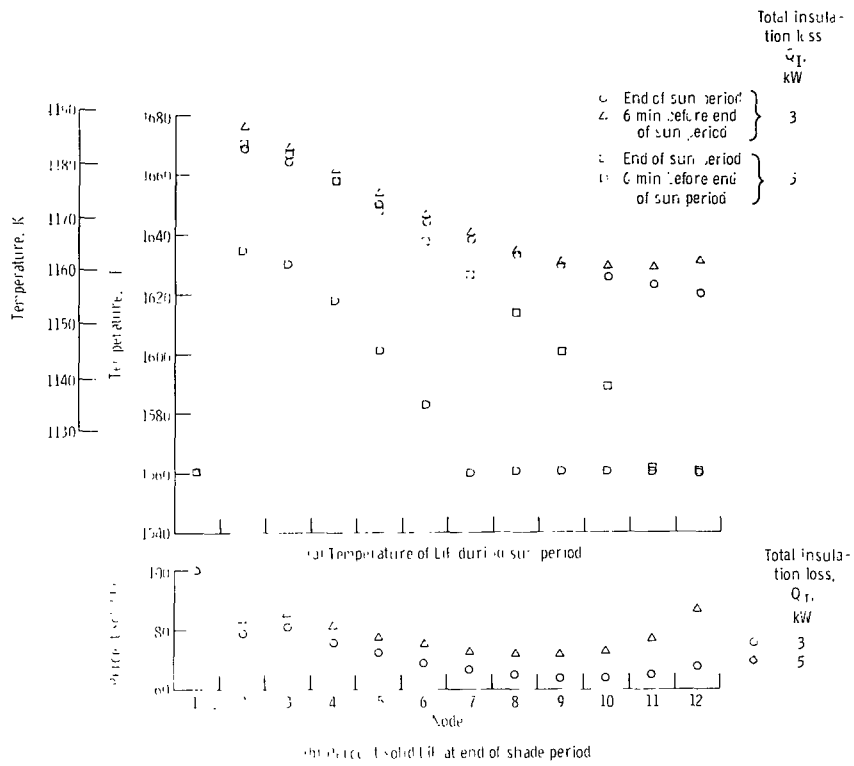


Figure 11 - Comparison of LIF for case given in figure 10

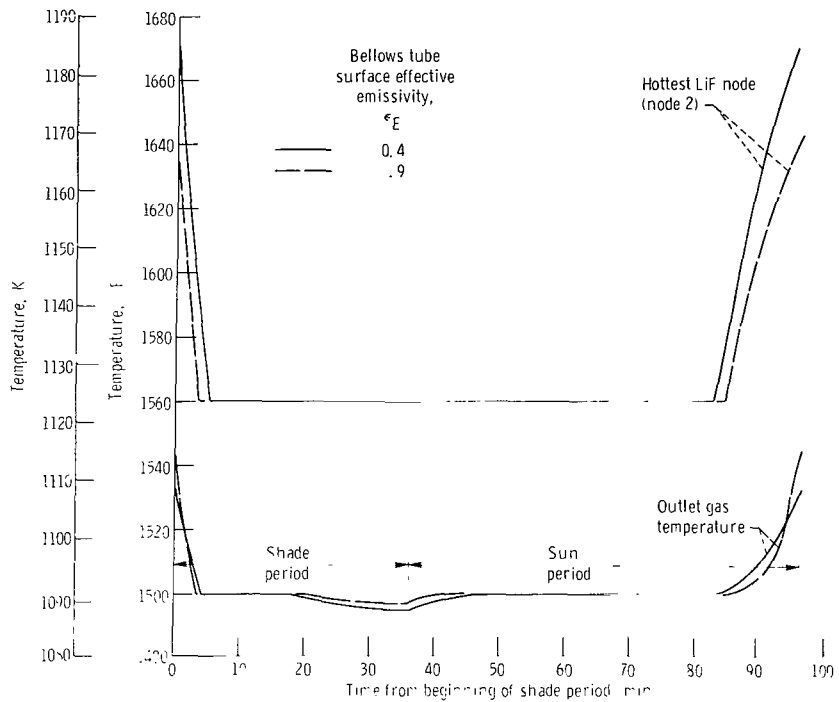


Figure 12 - Performance for 60-minute sun, 36-minute shade period orbit. Temperature of hottest node at which heat rejection doors begin to open, 1680 F (1139 K), temperature of hottest node at which heat rejection doors begin to close, 1650 F (1172 K), total insulation loss, 5 kilowatts; bellows tube surface effective solar absorptivity, 0.75

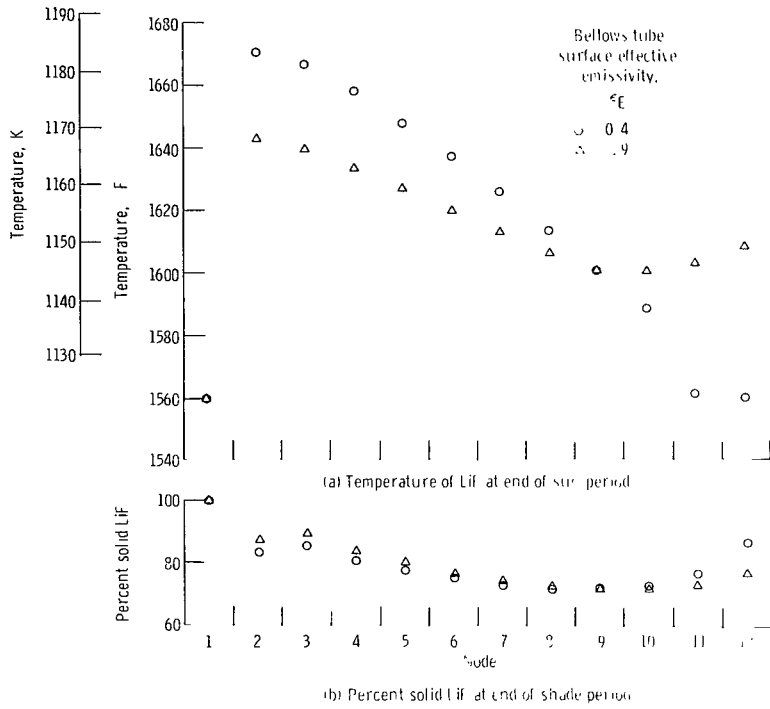


Figure 13. - Conditions of LiF for case given in Figure 12

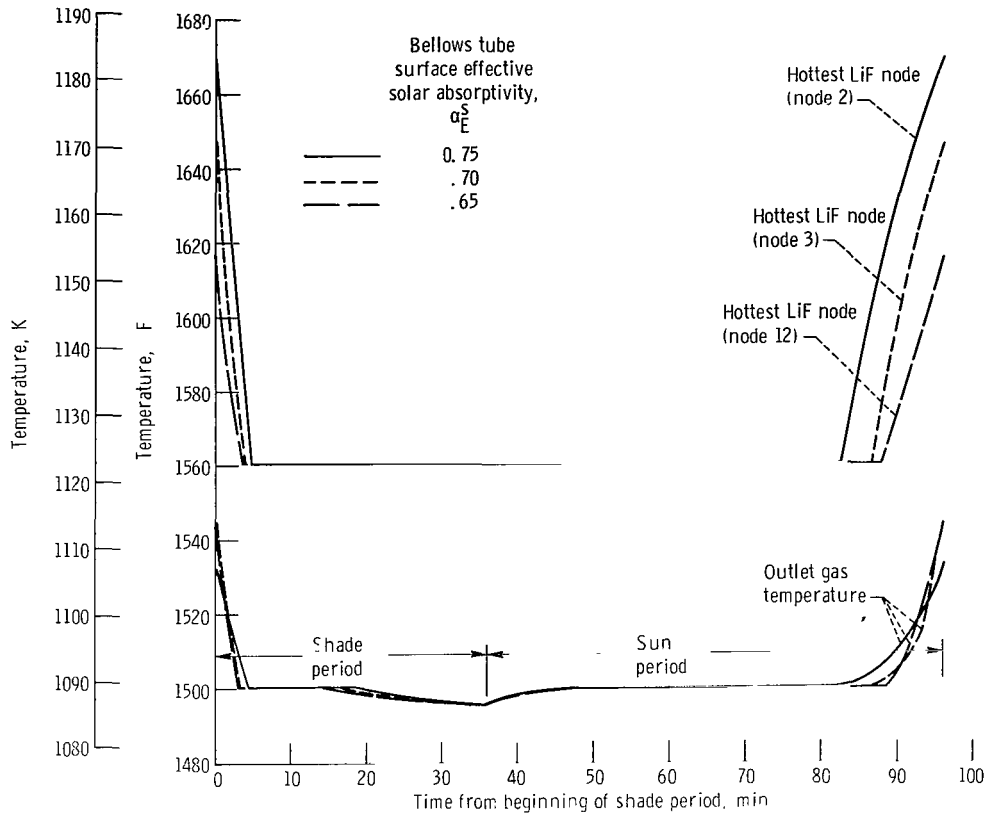


Figure 14 - Performance for 60-minute sun, 36-minute shade orbit. Temperature of hottest node at which heat rejection doors begin to open, 1680 F (1189 K); temperature of hottest node at which heat rejection doors begin to close, 1650 F (1172 K); total insulation loss, 5 kilo-atoms; bellows tube surface effective emissivity, 0.4.

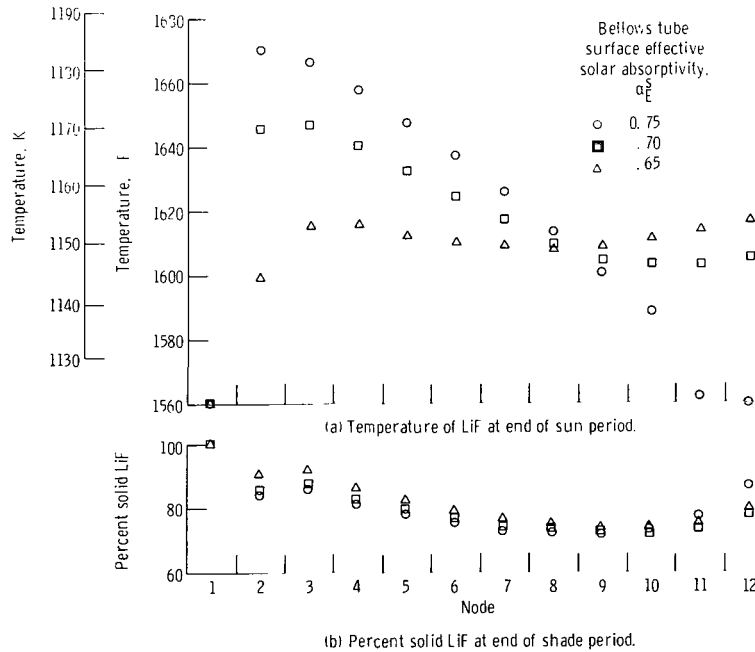


Figure 15. - Conditions of LiF for case given in figure 14.

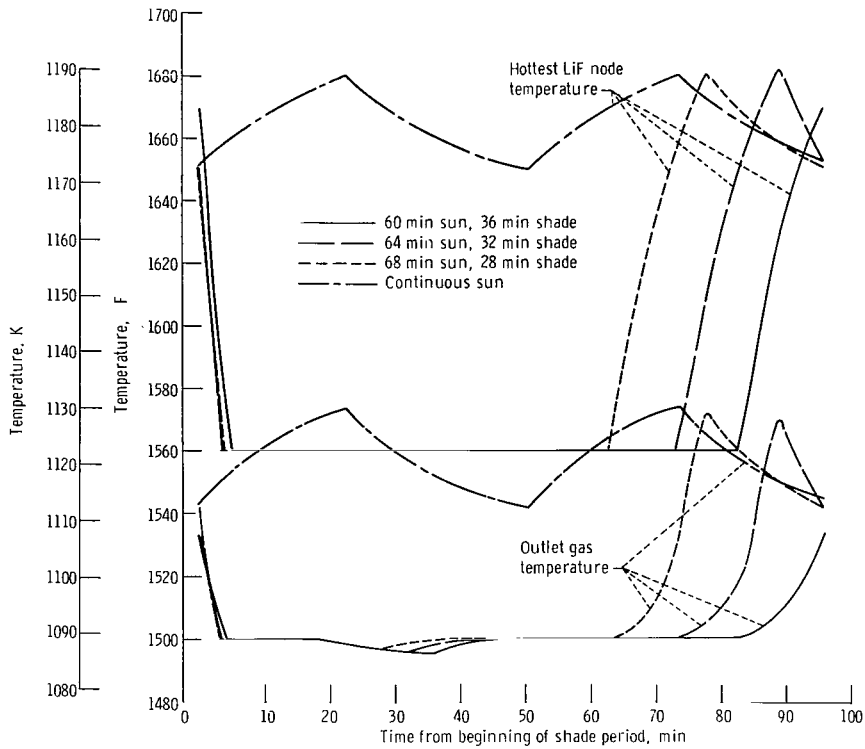


Figure 16. - Performance with variation in sun-shade times, 96-minute orbit. Temperature of hottest node at which heat rejection doors begin to open, 1680 F (1189 K); temperature of hottest node at which heat rejection doors begin to close, 1650 F (1172 K); total insulation loss, 5 kilowatts; bellows tube surface: effective emissivity, 0.4; effective solar absorptivity, 0.75.

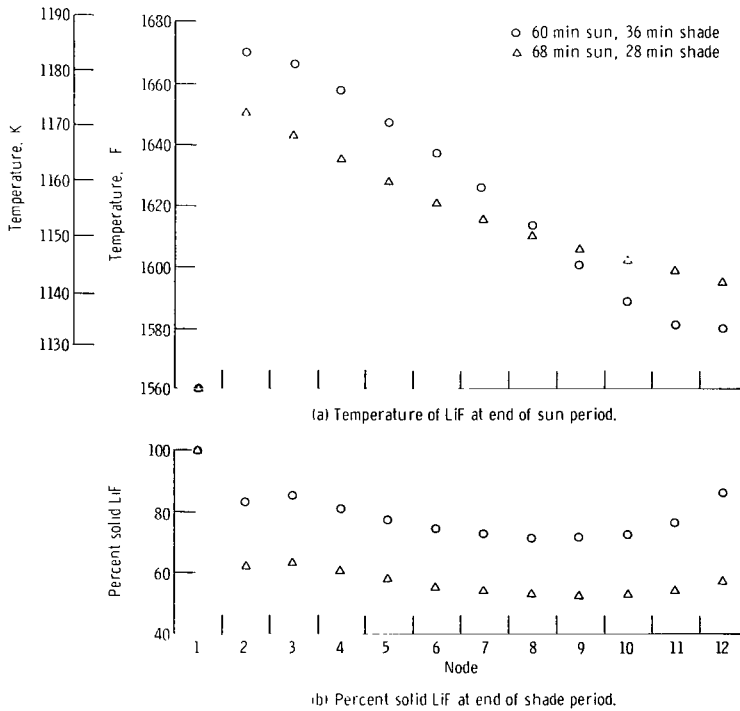


Figure 17. - Conditions of LiF for case given in figure 16.

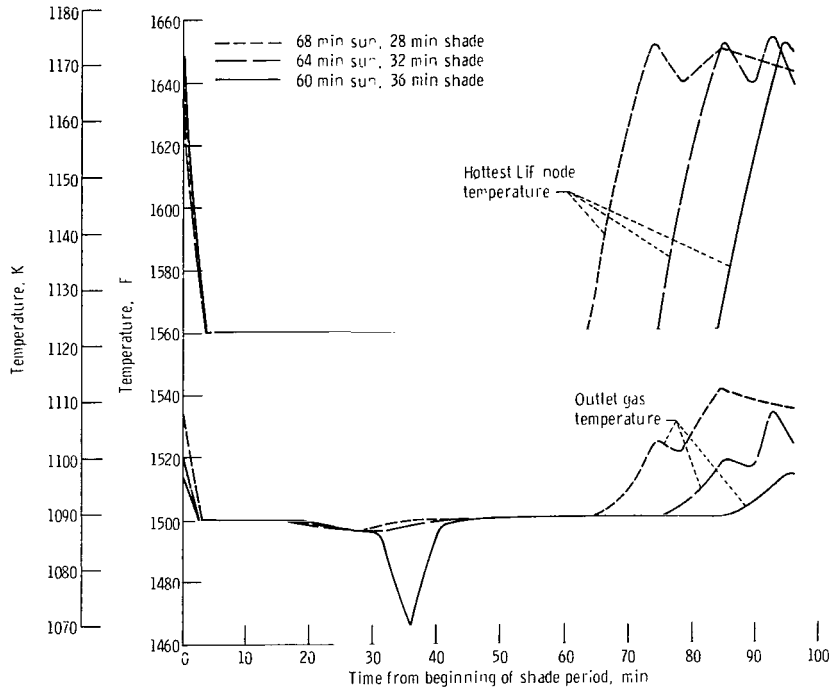


Figure 18. - Performance with variation in sun-shade times, 96-minute orbit. Temperature of hottest node at which heat rejection doors begin to open, 1650 F (1172 K); temperature of hottest node at which heat rejection doors begin to close, 1640 F (1167 K); total insulation loss, 5 kilowatts; bellows tube surface: effective emissivity, 0.4; effective solar absorptivity, 0.75

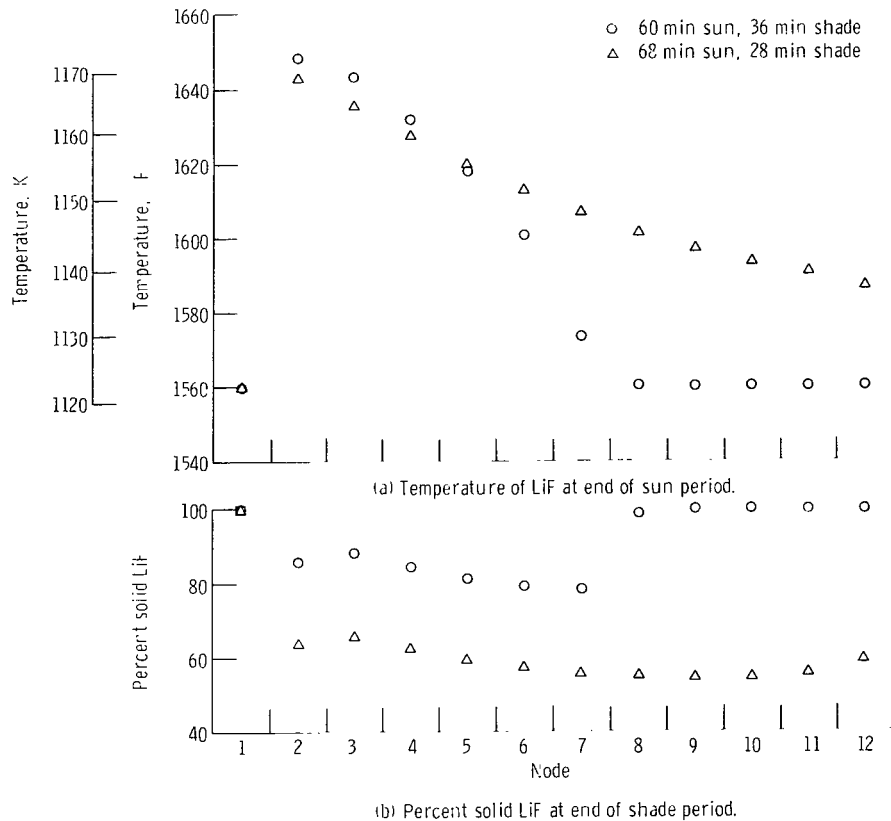


Figure 19. - Conditions of LiF for case given in figure 18.

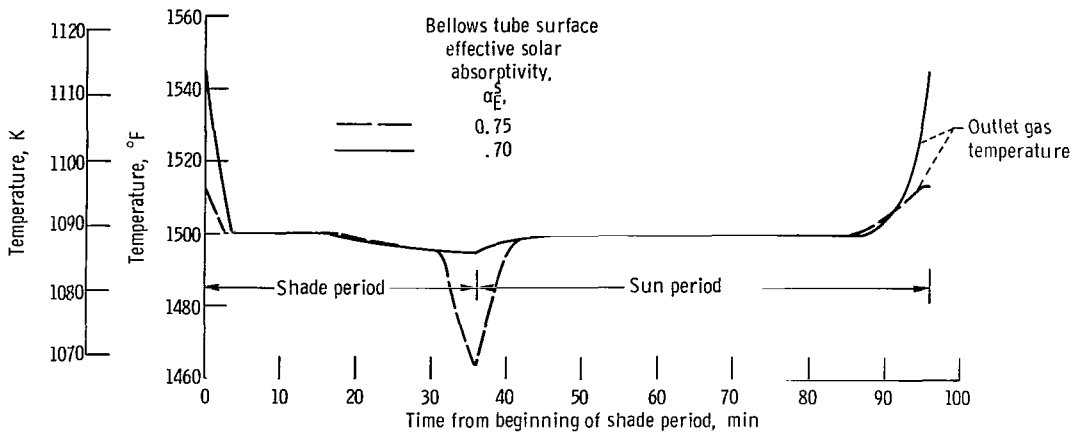


Figure 20. - Performance for 60-minute sun, 36-minute shade period. Temperature of hottest node at which heat rejection doors begin to open, 1650° F (1172 K); temperature of hottest node at which heat rejection doors begin to close, 1640° F (1167 K); total insulation loss, 5 kilowatts; bellows tube surface effective emissivity, 0.4.

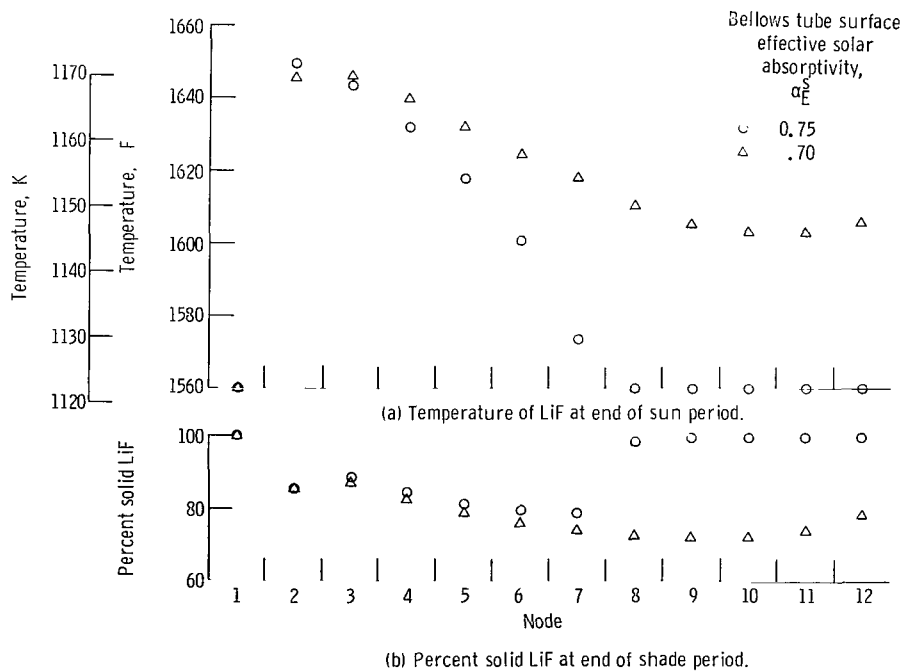


Figure 21. - Conditions of LiF for case given in figure 20.

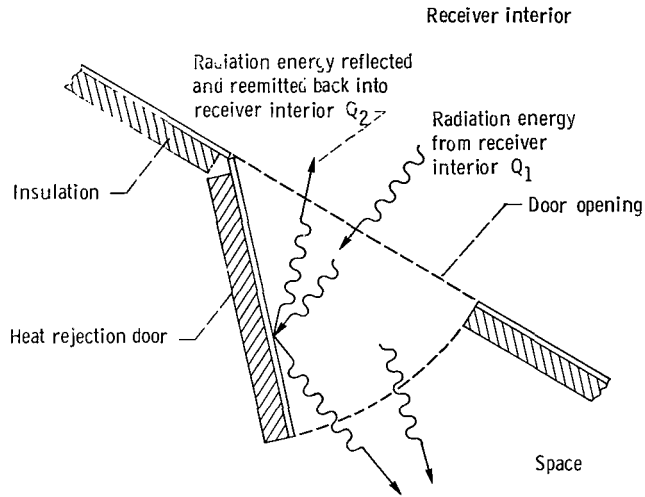


Figure 22. - Thermal model of heat rejection doors.

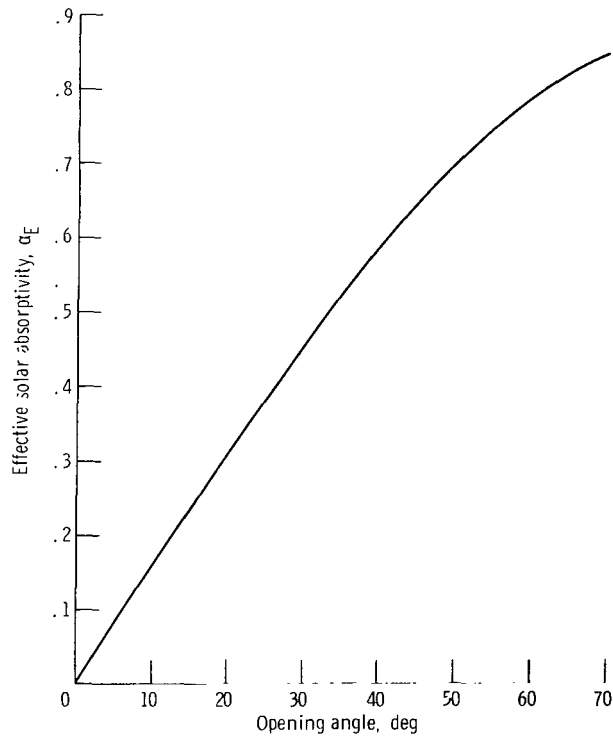


Figure 23. - Effective absorptivity of heat rejection door node plotted against opening angle.

NATIONAL AERONAUTICS AND SPACE ADMINISTRATION
WASHINGTON, D. C. 20546

OFFICIAL BUSINESS
PENALTY FOR PRIVATE USE \$300

FIRST CLASS MAIL



POSTAGE AND FEES PAID
NATIONAL AERONAUTICS AND
SPACE ADMINISTRATION

03U 001 28 51 3DS 71088 00903
AIR FORCE WEAPONS LABORATORY /WLCL/
KIRTLAND AFB, NEW MEXICO 87117

ATT E. LOU BOWMAN, CHIEF, TECH. LIBRARY

POSTMASTER: If Undeliverable (Section 158
Postal Manual) Do Not Return

"The aeronautical and space activities of the United States shall be conducted so as to contribute . . . to the expansion of human knowledge of phenomena in the atmosphere and space. The Administration shall provide for the widest practicable and appropriate dissemination of information concerning its activities and the results thereof."

— NATIONAL AERONAUTICS AND SPACE ACT OF 1958

NASA SCIENTIFIC AND TECHNICAL PUBLICATIONS

TECHNICAL REPORTS: Scientific and technical information considered important, complete, and a lasting contribution to existing knowledge.

TECHNICAL NOTES: Information less broad in scope but nevertheless of importance as a contribution to existing knowledge.

TECHNICAL MEMORANDUMS: Information receiving limited distribution because of preliminary data, security classification, or other reasons.

CONTRACTOR REPORTS: Scientific and technical information generated under a NASA contract or grant and considered an important contribution to existing knowledge.

TECHNICAL TRANSLATIONS: Information published in a foreign language considered to merit NASA distribution in English.

SPECIAL PUBLICATIONS: Information derived from or of value to NASA activities. Publications include conference proceedings, monographs, data compilations, handbooks, sourcebooks, and special bibliographies.

TECHNOLOGY UTILIZATION PUBLICATIONS: Information on technology used by NASA that may be of particular interest in commercial and other non-aerospace applications. Publications include Tech Briefs, Technology Utilization Reports and Technology Surveys.

Details on the availability of these publications may be obtained from:

**SCIENTIFIC AND TECHNICAL INFORMATION OFFICE
NATIONAL AERONAUTICS AND SPACE ADMINISTRATION
Washington, D.C. 20546**